A CENSUS OF MID-INFRARED SELECTED ACTIVE GALACTIC NUCLEI IN MASSIVE GALAXY CLUSTERS AT $0 \lesssim z \lesssim 1.3$

A Thesis

by

ADAM R. TOMCZAK

Submitted to the Office of Graduate Studies of
Texas A&M University
in partial fulfillment of the requirements for the degree of

MASTER OF SCIENCE

Approved by:

Chair of Committee,	Kim-Vy Tran
Committee Members,	Wolfgang Bangerth
	Casey Papovich
Head of Department,	George Welch

December 2012

Major Subject: Physics

ABSTRACT

We conduct a deep mid-infrared census of nine massive galaxy clusters at ($0 < z < 1.3$) with a total of ~ 1500 spectroscopically confirmed member galaxies using *Spitzer*/IRAC photometry and established mid-infrared color selection techniques. Of the 949 cluster galaxies that are detected in at least three of the four IRAC channels at the $\geq 3\sigma$ level, we identify 12 that host mid-infrared selected active galactic nuclei (IR-AGN). To compare the IR-AGN across our redshift range, we define two complete samples of cluster galaxies: (1) optically-selected members with rest-frame $V_{\rm AB}$ magnitude < -21.5 and (2) mid-IR selected members brighter than ($\rm M^*_{3.6}$+0.5), i.e. essentially a stellar mass cut. In both samples, we measure $f_{\rm IR-AGN}$ $\sim 1\%$ with a strong upper limit of $\sim 3\%$ at $z < 1$. This uniformly low IR-AGN fraction at $z < 1$ is surprising given the fraction of 24μm sources in the same galaxy clusters is observed to increase by about a factor of four from $z \sim 0$ to $z \sim 1$; this indicates that most of the detected 24μm flux is due to star formation. Only in our single galaxy cluster at $z = 1.24$ is the IR-AGN fraction measurably higher at $\sim 15\%$ (all members; $\sim 70\%$ for late-types only). In agreement with recent studies, we find the cluster IR-AGN are predominantly hosted by late-type galaxies with blue optical colors, i.e. members with recent/ongoing star formation. The four brightest IR-AGN are also X-ray sources; these IR+X-ray AGN all lie outside the cluster core ($R_{proj} \gtrsim 0.5$ Mpc) and are hosted by highly morphologically disturbed members. Although our sample is limited, our results suggest that $f_{\rm IR-AGN}$ in massive galaxy clusters is not strongly correlated with star formation at $z < 1$, and that IR-AGN have a more prominent role at $z \gtrsim 1$.

ACKNOWLEDGMENTS

We thank our referee, Ryan Hickox, as well as Paul Martini and David Atlee for their instructive comments and suggestions that improved our paper. We would also like to thank Pauline Barmby for assistance with the IRAC photometry, Julien Devriendt for providing template galactic SEDs, Ricardo Demarco for providing *HST* imaging of RDCS 1252 and Adam Muzzin for providing data on the 3.6μm luminosity function. K.T. acknowledges generous support from the Swiss National Science Foundation (grant PP002-110576). In this work we have made use of the kcorrect software originally developed by Mike Blanton [12] and adapted to Python by Taro Sato. This work is based on observations made by the *Spitzer Space Telescope* which is operated by the Jet Propulsion Laboratory, California Institute of Technology, under contract with the NASA. This research has made use of the VizieR catalogue access tool, CDS, Strasbourg, France.

NOMENCLATURE

AB	Absolute Bolometric
ACS	Advanced Camera for Surveys
AGES	AGN and Galaxy Evolution Survey
AGN	Active Galactic Nucleus
CMD	Color-Magnitude Diagram
CMR	Color-Magnitude Relation
ELG	Emission Line Galaxy
HST	Hubble Space Telescope
ICM	Intra-Cluster Medium
IR	Infrared
IRAC	Infrared Array Camera
kpc	Kiloparsec
ΛCDM	Lambda Cold Dark Matter
MIPS	Multiband Imaging Photometer for *Spitzer*
Mpc	Megaparsec
NOAO	National Optical Astronomy Observatory
PAH	Polycyclic Aromatic Hydrocarbon
PSF	Point Spread Function
SDSS	Sloan Digital Sky Survey
SED	Spectral Energy Distribution
SSP	Singal Stellar Population
(U)LIRG	(Ultra) Luminous Infrared Galaxy
WFPC-2	Wide Field and Planetary Camera 2
WISE	Wide-field Infrared Survey Explorer

TABLE OF CONTENTS

Page

LIST OF TABLES

LIST OF FIGURES

FIGURE Page

1. INTRODUCTION

Our understanding of galaxy evolution in dense cluster environments continues to improve as observations broaden in wavelength and redshift range. One fundamental observation is that dense environments at low redshifts are dominated by passive, early-type galaxies that define a narrow red sequence in an optical color-magnitude diagram [86][13][50], and studies of the cluster color-magnitude relation (CMR) show that the luminous red sequence members in galaxy clusters have not evolved significantly since $z \sim 0.8$ [84]. In contrast, the less massive cluster members continue to migrate to the red sequence as studies at $z > 0.6$ show there are fewer faint red galaxies in clusters compared the field and to lower redshift clusters [21][90][84]. Recent observations at $z > 1.4$ have now even found massive, star forming galaxies in clusters [95][49].

The question then remains as to what halts star formation in cluster galaxies? Possible environmental processes include ram-pressure stripping [45], tidal effects from the cluster potential [35], and galaxy-galaxy interactions [81], but none are completely effective at reproducing the star formation histories and scaling relations observed in galaxy clusters. One model that has proven successful is including feedback from active galactic nuclei (AGN). Semi-analytic models that include AGN are able to reproduce observed mass/luminosity functions [18][14][62]. AGN can also affect the intra-cluster medium (ICM) where models find that including AGN produces much better agreement with observations of X-ray properties of the ICM [15][79][69].

AGN feedback seems to be the ideal solution to resolve many outstanding discrepancies between models and observations [40][39][91]; however, there is not yet clear observational evidence that AGN contribute significantly to the quenching of star formation in cluster galaxies, making clusters into resting homes of passive galaxies. Several groups using primarily X-ray observations find the fractional density of X-ray selected active galactic nuclei (X-ray AGN) in cluster environments increases with

redshift [32][68]. Similarly, using X-ray, infrared and radio selection at $z < 1.5$ [41] find that the AGN surface-density (N/arcmin^2) is greater for clusters than in the field and that the AGN volume-density (N/Mpc^3) for clusters increases with redshift. In contrast, a study of CL $0023+04$, a large scale system of four galaxy groups merging at $z \sim 0.83$, does not find an excess of X-ray sources relative to the field [59]. In general, studies are hampered by the small number of X-ray AGN and the need to isolate a large sample of cluster galaxies at higher redshifts. Another important issue is that different diagnostics select different populations of AGN [46][48][44] and so no single approach will be complete. Thus while CL $0023+04$ does not have an excess of X-ray sources, [64] does find a population of passive (no detectable Hα) members with [OII] emission that may be due to AGN.

With the launch of the *Spitzer Space Telescope*, mid-infrared selection has become an efficient alternative method for identifying AGN that complements existing X-ray, radio, and optical search techniques. Note that mid-IR color selection is particularly effective at selecting high-Eddington AGN (e.g. [48][53]). A single stellar population (SSP) has a declining Rayleigh-Jeans tail that longward of 1μm makes these type of SEDs blue in the mid-infrared [100] while an SED with an active galactic nucleus has a rising power law [33] and so will be red. Advantages of selecting with mid-infrared wavelengths include decreased attenuation from dust and sensitivity to AGN spanning a broad range in redshift ($0 < z \lesssim 2$ [89][61]). In the mid-IR, red colors are due to thermal emission from heated dust, either by radiation from stars or an active nucleus, and so dust heated by young stellar populations, e.g. ultra-luminous infrared galaxies (ULIRGs), can contaminate a mid-IR selected AGN sample [27]. However, (U)LIRGs are extremely rare in massive galaxy clusters with only one confirmed ULIRG out of thousands of known cluster galaxies at $z < 1$ [85][17].

We expect that most cluster galaxies will populate a tight distribution in mid-IR color space because massive galaxies in clusters formed the bulk of their stars at $z > 2$ and have evolved passively since [13][97][94][76]. However, if AGN are

essential for quenching star formation in cluster galaxies, the AGN fraction should increase with redshift because the IR luminosity function and fraction of star forming galaxies in massive clusters increases by a factor $\gtrsim 4$ from $z \sim 0$ to $z \sim 1$ [85][4]. We can identify AGN using mid-IR colors to determine if the IR-AGN fraction evolves with redshift and, combined with known X-ray AGN, also study the properties of cluster AGN to obtain a more complete picture of AGN in galaxy clusters. Note that selecting AGN with optical diagnostics becomes quite challenging at $z > 0.4$ because key spectral features shift into the near-infrared, and extremely deep radio observations are significantly more time intensive than mid-IR imaging.

Motivated by these issues, we present the first extensive mid-infrared census of massive galaxy clusters at $0 < z < 1.3$. Our clusters are the most massive systems known ($M_{\rm vir} \gtrsim 5 \times 10^{14} M_{\odot}$) having comprehensive spectroscopic information for member galaxies as well as deep optical photometry (see §2.2) and so provide the most representative sample of galaxy clusters in the range $0 \lesssim z \lesssim 1.3$. This paper is organized as follows in §2 we discuss the reductions of the *Spitzer* mid-infrared and optical data for each cluster. In §3 we describe how we select AGN and results for each cluster. In §4 we measure the IR-AGN fraction as a function of redshift and discuss properties of their host galaxies, and we present our conclusions in §5. All magnitudes are in the AB system unless otherwise noted. We assume a ΛCDM cosmology throughout with $\Omega_M = 0.27$, $\Omega_\Lambda = 0.73$ and $h = 0.71$

2. DATA AND REDUCTIONS

2.1 Spitzer IRAC

Mid-infrared observations were taken with the IRAC instrument [37] on board the *Spitzer Space Telescope* [99] and are publicly available on the Spitzer archive. IRAC observes in four mid-infrared channels centered at 3.6, 4.5, 5.8 and 8.0 μm. These channels have transmission functions such that all emission between 3.1 and 9.4 μm will be detected. Furthermore, the edges of the channels are steep, so that as an emission feature becomes redshifted out of one bandpass it will promptly shift into the adjacent one. This ensures that spectral features (such as PAH emission from dusty star formation) can be traced fairly easily over a wide range in redshift.

For most of the cluster fields (Table 2.1), multiple IRAC observations were conducted at different times. In the interest of increasing depth we make use of all available data. This also frequently served to increase the area of coverage allowing more cluster galaxies to be detected.

2.1.1 Mosaicking

Each observational campaign is composed of a series of dithered images referred to as Basic Calibrated Data (BCD). The depth of a final mosaic depends on the combination of exposure time and number of frames per sky position. BCDs are single-frame images that have been reduced and flux-calibrated on a basic level by the *Spitzer* pipeline. We performed further processing and mosaicking using MOPEX(18.3 rev 1, [66]), a set of reduction and analysis tools designed by the *Spitzer Science Center*. The software includes modules that flag and remove spurious detections that are not accounted for in the automatic pipeline reduction. Prior to mosaicking, images were inspected for artifacts such as muxbleed and column pull-up/down and were mitigated using the *cosmetic* module from MOPEX.

Table 2.1
Cluster Properties

Cluster	RA Dec[a]	z-Range[b]	N_z [c]	$N_{\rm IRAC}$ [d]	$\log(L_X)$[e]	Status[f]
Coma	12 59 35.7 +27 57 34	(0.013 - 0.033)	348	262	43.0	Relaxed
Abell 1689	13 11 29.5 −01 20 17	(0.17 - 0.22)	81	73	43.3	Relaxed
MS 1358+62	13 59 50.4 +62 31 03	(0.315 - 0.342)	171	133	43.0	Unrelaxed
CL 0024+17	00 26 35.7 +17 09 43	(0.373 - 0.402)	205	75	42.5	Unrelaxed
MS 0451−03	04 54 10.9 −03 01 07	(0.52 - 0.56)	242	90	43.3	Relaxed
MS 2053−04	20 56 21.3 −04 37 51	(0.57 - 0.60)	132	87	42.8	Unrelaxed
MS 1054−03	10 57 00.0 −03 37 36	(0.80 - 0.86)	153	120	43.2	Unrelaxed
RX J0152−13	01 52 43.9 −13 57 19	(0.81 - 0.87)	147	80	43.3	Unrelaxed
RDCS J1252−29	12 52 54.4 −29 27 18	(1.22 - 1.25)	38	29	42.8	Unrelaxed

All clusters in this sample have $M_{\rm vir} \gtrsim 5 \times 10^{14} M_\odot$.
[a] Right ascension and Declination are for J2000.
[b] Range of redshifts for spectroscopically confirmed members from [85] and [23].
[c] Total number of spectroscopically confirmed cluster members. Redshifts are from [82](Coma), [30](Abell 1689), [38](MS 1358), [73](CL 0024), [74](MS 0451), [92](MS 2053), [94](MS 1054), [22](RX J0152) and [23](RDCS J1252) respectively.
[d] Number of cluster galaxies with detections in at least three IRAC channels.
[e] Bolometric ICM X-ray luminosities (ergs $\rm s^{-1}$) from [51](Coma, MS 1358, MS 2053, MS 1054, RX J0152), [5](A1689), [25](MS 0451), [101](CL 0024) and [83](RDCS J1252).
[f] Dynamical state of each cluster, determined from redshift distributions and X-ray & weak lensing profiles. Unrelaxed systems are those that show signs of a cluster scale merger.

Overlapping is another necessary step in the image reduction process available as a package in MOPEX. Within a set of dithered frames, the individual backgrounds may vary to the point that the background of a final mosaic shows a checkered pattern/gradient. Performing overlap matches the backgrounds of all input frames and so removes this effect. After overlapping, BCDs are then stacked. Weight maps were also obtained for each mosaic as coverage varied between campaigns.

2.1.2 Photometry and Completeness

Fixed-aperture photometry was carried out on each mosaic using SExtractor 2.5.0 [8]. In order to analyze cluster galaxies at varying z equally, apertures were chosen at constant proper sizes according to cluster redshifts (except for Coma, see §3.2.1). Ideally, apertures should be small so as to isolate the central engine and reduce possible contamination from, e.g. extended star forming regions in the host galaxy. However, the IRAC point spread functions (PSFs) are ∼1.66, 1.72, 1.88 and 1.98" in diameter for channels 1−4 respectively, and fluxes determined from apertures comparable to the IRAC pixel size ($\sim 1.22''$ px^{-1}) are subject to sampling errors. These caveats constrain the minimum size of a reasonable aperture. Ultimately, we choose a radius of ∼12.6 kpc, which corresponds to an aperture diameter of 3" for the most distant cluster (see Table 2.2 for all aperture sizes). We note that a 12.6 kpc aperture is much larger than would be "ideal" for this type of a study; however, we feel that accepting this limitation is preferred over varying the physical sizes of apertures, which would likely introduce a selection bias.

Aperture corrections were determined from IRAC calibration stars [80] as discussed in [2], except for Coma where theoretical aperture corrections for extended sources were used. Although some galaxies in our other low-z clusters are resolved, the discrepancy between extended- and point-source aperture corrections is not enough to affect our results. Further discussion regarding these corrections can be found in the IRAC Instrument Handbook. IRAC fluxes are calibrated based

Table 2.2
IRAC Photometry

Cluster	Aperture [a]	3.6μm[b]	4.5μm[b]	5.8μm[b]	8.0μm[b]
Coma	15"	20.3	20.1	18.8	18.1
1689	7.7"	19.6	19.9	19.7	19.0
1358	5.3"	20.8	21.1	20.4	20.2
0024	4.8"	20.6	20.9	20.2	20.0
0451	4.0"	20.9	21.0	20.3	20.0
2053	3.8"	20.8	20.9	20.3	20.1
1054	3.3"	21.1	21.2	20.7	20.5
0152	3.3"	21.1	21.4	20.1	20.3
1252	3.0"	21.0	21.3	20.6	20.6

[a] Fixed circular aperture corresponding to physical diameter of ~ 25 kpc at cluster redshift except for Coma where the aperture corresponds to 6 kpc ; see §3.2 for more details.
[b] AB magnitude corresponding to 80% completeness limit; see §2.1.2 for more details.

on 24″ (diameter) apertures and an appropriate correction needs to be applied to photometry using apertures of different sizes. Aperture corrections are defined as the difference between the magnitude of a point-sources from a 24″ aperture and the magnitude from the aperture of interest. We determined aperture corrections from five standard stars (HD-165459, 1812095, KF06T1, NPM1p66.0578, NPM1p67.0536) using the average as the final value. Because Galactic extinction is negligible at these wavelengths ($\lesssim 0.01$ mag) the corrections are less than the measurement uncertainties, we do not correct the IRAC magnitudes; however, we do correct for Galactic extinction in the optical filters.

Completeness was measured using the *gallist* and *mkobjects* modules in IRAF[1]. For each mosaic, 1000 artificial galaxies in half-magnitude bins between $16 \leq m \leq 25$ were distributed randomly. Source extraction was then carried out for these fake sources with identical parameters as used for the real sources. Fake sources that were extracted with magnitudes brighter than their input value were discarded as instances of blending. In order to get a sense of the completeness within each cluster, sources were added in 1.5×1.5 Mpc boxes centered on the core of each cluster. Measurements of completeness are shown in Figure 2.1 and Table 2.2.

In performing source matching, we start with the coordinates of a galaxy from optical images. We then search for the nearest source in each IRAC catalog within a 2" radius, i.e. slightly larger than the IRAC PSF. In a few cases, e.g. in the cores of the high redshift clusters, there is some blending of IRAC sources. We deblend and separate sources using the SExtractor parameters DEBLEND NTHRESH=64 (for all channels) and DEBLEND MINCONT=0 and 0.005 (for channels 1,2 and 3,4 respectively). Visual inspection confirms that these parameters are effective at deblending sources with only 2 pairs/groups of galaxies still blended in the $z > 0.8$ clusters; only one of these has an IR-AGN signature (see §3.2.8).

[1]IRAF is distributed by the National Optical Astronomy Observatory (NOAO), which is operated by the Association of Universities for Research in Astronomy, Inc., under cooperative agreement with the National Science Foundation.

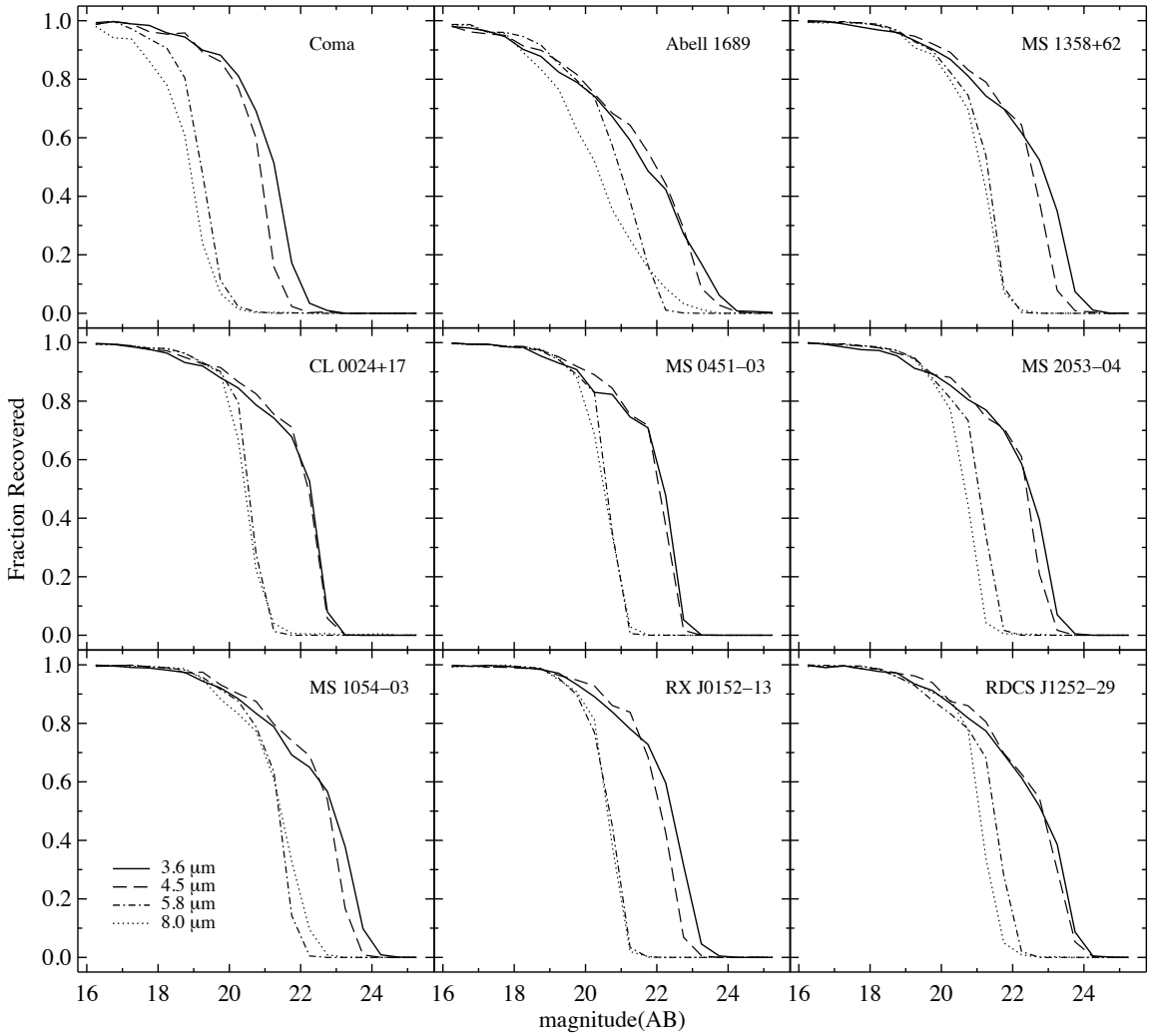

Fig. 2.1. Completeness functions for each cluster field showing the fraction of recovered sources versus their input magnitude. For each cluster, 1000 generated galaxies were randomly distributed in 0.5 magnitude bins in a 1.5×1.5 Mpc^2 box centered near the cluster core. Sources that were extracted with magnitudes brighter than their input value were rejected as instances of blending. The 3.6 and 4.5μm channels exhibit a more gradual decline in completeness due to source confusion from greater crowding [7] which increases the likelihood of blending.

2.2 Optical Photometry and Spectroscopy

Catalogs of optical and near infrared photometry as well as optical spectroscopy were obtained from multiple sources. Observed photometry was converted to rest-

frame values using KCorrect v0.2.1, an extension of *kcorrect* [12] developed for Python by Taro Sato. Extensive spectroscopic catalogs were used to confirm membership for each cluster. General properties of each galaxy cluster are shown in Table 2.1. To summarize:

- *Coma*: Photometry was taken from [71] which consists of measurements in the B and R bands. Completeness was assessed to be 22.5 mag and 21 mag in B and R respectively. Spectroscopy for the Coma cluster was taken as part of the Cluster and Infall Nearby Survey (CAIRNS: [82]). Galaxies targeted in this survey were selected from digitized images of the POSS I 103aE (red) plates which are complete down to E=15-16.

- *Abell 1689*: Data for Abell 1689 [30] were taken as follow-up to the photometric observations conducted by [31]. Photometry was acquired for the BVR bands and is complete to 23.0, 22.7 and 22.7 mag respectively. Spectra were obtained for most($\sim$75%) of the photometric cluster members at $R \leq 17.75$ mag which drops to $\sim$40% at $R \leq 19.5$ mag.

- *MS 1358+62*: Observations of MS 1358 taken from [38] including photometry in the V and R bands and spectroscopy. Spectroscopic completeness was determined to be >80% at $R \leq 21$ mag when compared to photometric observations which were complete to $R \sim 23.5$ mag.

- *CL 0024+17 and MS 0451-03*: Data for CL 0024 and MS 0451, including photometry from the HST WFPC2 instrument, are discussed in detail in [96] and [73][74]. Photometry was measured to be complete to $I \sim 25$ (Vega mags)^2 for CL 0024 and spectroscopic completeness was found to be $> 65\%$ at $I < 21.1$ and $I < 22.0$ mag for CL 0024 and MS 0451 respectively. Additional ground-based photometry was also obtained in the $BVRIJK_s$ bands reaching

3σ depths of 27.8, 26.9, 26.6, 25.9, 21.6 & 19.7 mag for CL 0024 and 28.1, 27.0, 27.3, 25.9, & 20.2 mag for MS 0451 [75].

- *MS 2053-04 and MS 1054-03*: Spectroscopy for MS 2053 is detailed in [92] and completeness determinations were assessed according to sampling and success rates. The success rate is defined as the number of spectroscopic redshifts obtained divided by the number of spectroscopic targets. Spectroscopic completeness was determined to be $\sim$70% at $m_{814} < 22$ mag. Similar methods were applied for MS 1054 [94] which found completeness to be >75% at $m_{814} \leq 21.2$ mag. Photometry for both MS 2053 and MS 1054 were acquired from the *HST*/WFPC-2 F606W and F814W filters.

- *RX J0152-13 and RDCS J1252-29*: Photometry for RX J0152 [11] was obtained from the ACS instrument onboard the *HST* in the F625W, F775W and F850LP bandpasses. Incompleteness for these observations begins to set in at $\sim$23.5, 22.5 and 22. [22] determined spectroscopic membership for RX J0152 confirming 102 cluster galaxies out of 262 targets. Observations of RDCS 1252 is outlined in [23]. Photometry was taken in the $BVRi_{775}z_{850}JK_s$ filters reaching 5σ limiting magnitudes of 26.5 & 26 mag in the J & K_s filters respectively. The spectroscopic success rate for RDCS J1252 was found to show a rapid decline at $K_s = 21.5$ mag, dropping from 85% to 20%.

[2]Here the I-band refers to the F814W filter from the WFPC-2 instrument

3. RESULTS

3.1 IRAC Color Selection of AGN

Mid-IR emission from an AGN is widely accepted as thermal continuum from circumnuclear dust [1][60]. As radiation from the accretion disk bombards the surrounding dust, it is heated to temperatures in the range of $\sim 20 - 1000$ K (below dust sublimation at $T \sim 2000$ K, [87]). IRAC colors alone can be an effective method for separating star forming galaxies from those hosting AGN at redshifts up to $z \sim 2$ [61][89]. It is worth noting that $\gtrsim 50\%$ of a galaxy's mid-IR emission must originate from the nuclear component [47][53][3] in order to be selected by the criteria of [89]. Thus, due to various limitations in measuring IRAC fluxes in our sample, we are only able to select galaxies that are dominated by AGN emission in the mid-IR.

The optical to mid-IR spectral energy distribution (SED) of AGN are typically well characterized by a rising power law with a few notable PAH features, thus causing these objects to appear increasingly red in the IRAC window [77]. Consequently, AGN tend to populate a separate region in mid-IR color space. Furthermore, studies have shown that various types of Seyferts have very similar mid-IR properties ([42] and references therein). Radiation at these wavelengths is relatively insensitive to extinction and thus gives a reliable measure of reprocessed emission from the central engine. However, it is worth noting that highly obscured sources ($A_V \gtrsim 30$) may be pushed outside the IRAC selection wedge (see Fig. 1 of [47]).

Figure 3.1 shows the empirical color selection criteria from both [89] and [61] for all IRAC sources detected in our nine cluster fields (including the cluster galaxies). Included in Figure 3.1 are color tracks of template galaxy SEDs from [24]: M82 (local starbursting galaxy; blue), VCC 1003 (local passively evolving galaxy; red), Mrk231 (Seyfert 1 AGN; black), and a Seyfert 2 template (pink). Tracks begin at $z = 0$ marked with Xs and go to $z = 2$ [77]. We refer the reader to [6] and [27] for a more

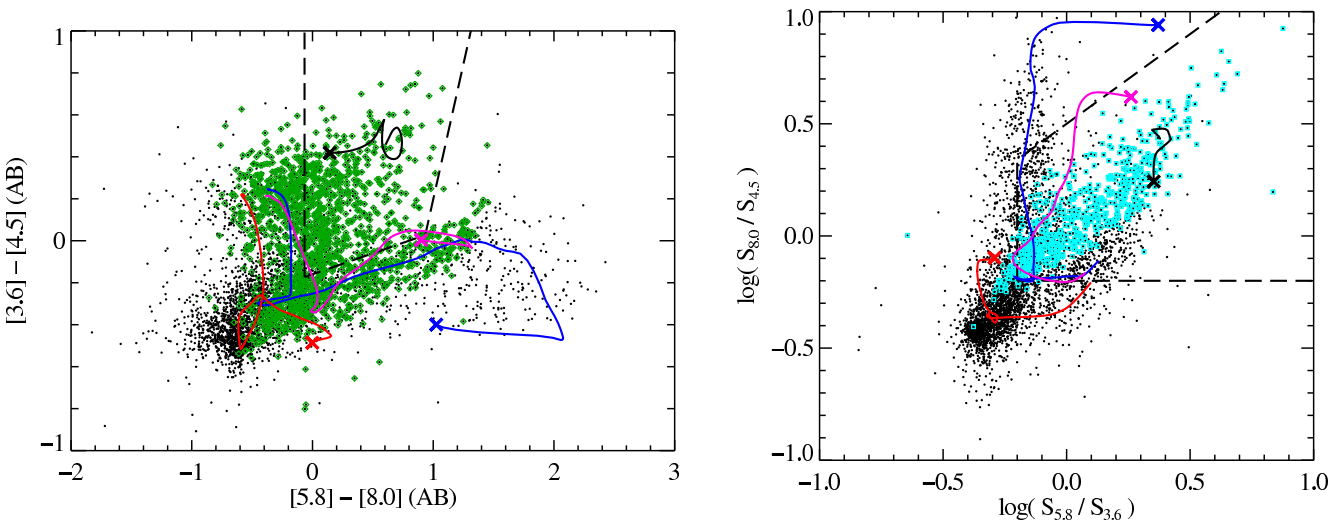

Fig. 3.1. Combined IRAC color-color plots as defined by Stern et al. (2005; left) and Lacy et al. (2004; right) derived from 3" apertures. Plotted are all detected sources in the IRAC mosaics for each cluster field. Curves in both panels are redshift-tracks for M82 (a local starbursting galaxy; blue), VCC 1003 (a local passively evolving galaxy; red), Mrk231 (Seyfert 1 AGN; black) and a Seyfert 2 template (pink); tracks begin at $z = 0$ marked with Xs and go to $z = 2$ [24][77]. The areas enclosed by the dashed lines are empirically defined regions designed to select galaxies dominated by emission from an AGN. Sources that fall in the wedge on the *left* are overlaid with cyan squares on the *right* whereas sources in the wedge on the *right* are overlaid with green diamonds on the *left*. Only ∼33% of Lacy IR-AGN are selected as Stern IR-AGN, whereas ∼89% of Stern IR-AGN are selected as Lacy IR-AGN. Furthermore, the Stern criteria determine an AGN fraction of 15%, whereas using the Lacy criteria it is 40%. We adopt the Stern IR selection for our analysis as it seems to suffer less contamination from non-AGN sources. See [6] and [27] for a more in depth analysis of mid-IR color evolution in galaxies with and without AGN.

detailed discussion of the mid-IR color evolution for galaxies including limitations of mid-IR selection.

To compare the selection methods of [61] and [89] we determine IR-AGN fractions for all galaxies (field and cluster) detected in all four bands of our IRAC imaging. We obtain fractions of 40% and 15% for the Lacy and Stern criteria respectively. In Figure 3.1, the green diamonds in the Stern plot correspond to sources that are selected as AGN using the Lacy criteria, whereas cyan squares in the Lacy plot cor-

respond to sources that are selected as AGN using the Stern criteria. Approximately 89% of the Stern-selected AGN are Lacy-selected AGN; however, the reverse shows that only ∼33% of all Lacy-selected AGN are also selected based on the Stern criteria. The higher IR-AGN fraction measured using the Lacy criteria is not surprising given that the track for M82 falls in the Lacy wedge. Because the Lacy criteria do not exclude starburst galaxies as effectively as the Stern criteria, we adopt the Stern criteria throughout the rest of this paper.

3.2 Individual Clusters

IRAC color plots for the nine massive galaxy clusters are shown in Figure 3.2. Only galaxies that have been spectroscopically confirmed as members with $\geq 3\sigma$ detections in at least 3 IRAC channels are shown. Data points indicate morphologically classified elliptical/S0 galaxies (red circles), late-type galaxies (blue diamonds), unclassified/merger (black circles), sources with no detection in channel 4 only (pink arrows) and no detection in channel 3 only (green arrows). For sources that lacked detections in a single bandpass, upper/lower limits were determined by assuming the 80% completeness magnitude for the respective bandpass (Table 2.2). Applying these limits mostly reveals a fainter population of passive galaxies. Considering that channels 1 & 2 (shorter wavelength) probe to fainter magnitudes than channels 3 & 4 (longer wavelength), galaxies in the "passive cloud" (with declining mid-IR SEDs) tend not to be detected at longer wavelengths while galaxies with IR-AGN (with increasing mid-IR spectra) are more likely to be detected in all four channels. This is why no potential candidate AGN are identified by our limit determinations. We use optically-determined coordinates for cluster galaxies to locate their IRAC counterparts. Using a matching radius of 2" (6" for Coma) we find the rate of detecting a false positive to be $< 1\%$.

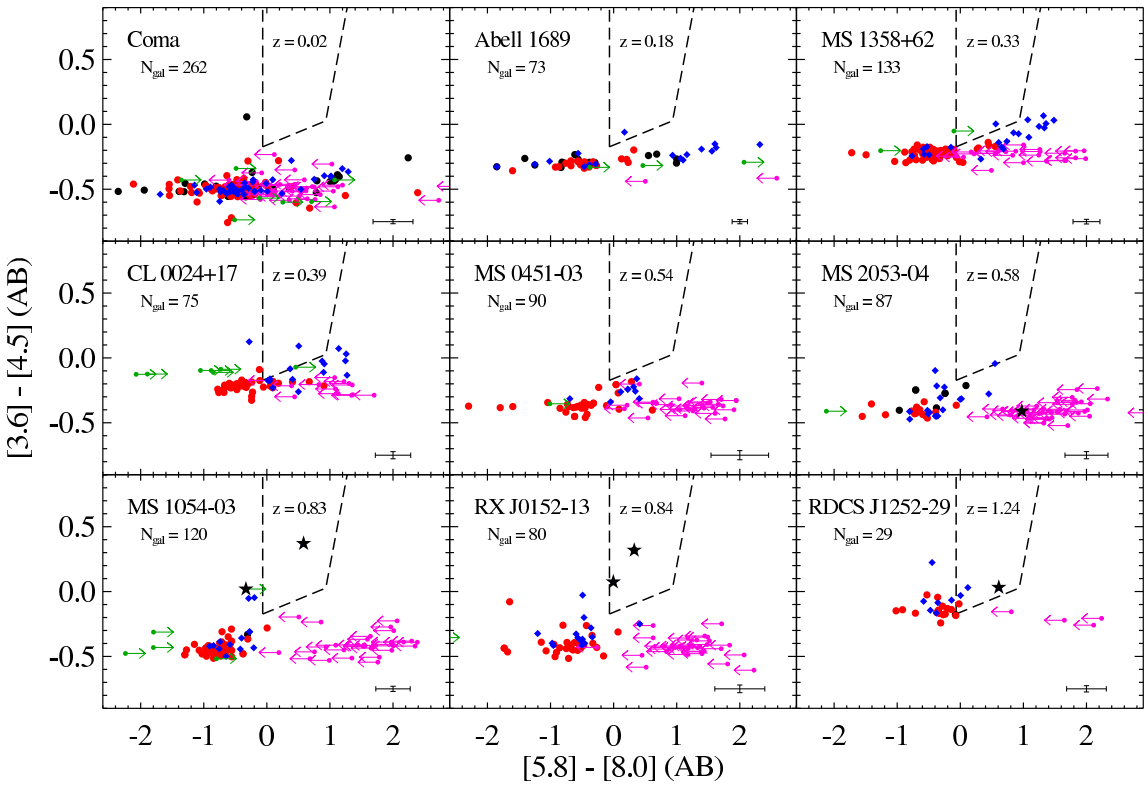

Fig. 3.2. IRAC color-color plots used to select active galactic nuclei (IR-AGN [89]) for the galaxy clusters in our study. Cluster redshift and number of confirmed members are shown in each panel. Data points correspond to morphologically classified early-type members (red circles), late-types (blue diamonds) and unclassified/mergers (black circles). Upper limits are determined for galaxies lacking detections in a particular channel (green and pink arrows, see §3). X-ray sources are indicated as stars. Mean uncertainties are shown in the lower-right corner of each panel. Early-type galaxies with blue IRAC colors populate the lower-left region in each plot (the "passive cloud") whereas IR-AGN populate the area enclosed by the dashed lines. Our cluster IR-AGN are predominantly hosted by late-type galaxies.

3.2.1 Coma

The Coma cluster is one of the richest and most closely studied galaxy clusters and is known to be dominated by passively evolving systems with early-type morphologies [70]. IRAC imaging for this cluster in all four channels covers roughly a 51.1'×62.5' region centered on NGC 4874, a field of view that includes 348 spectroscopically confirmed cluster galaxies from the CAIRNS [82]. Determining photome-

try with *Spitzer* data for resolved galaxies is not as straightforward as for the mostly unresolved galaxies in the distant clusters (see the IRAC Instrument Handbook for details). We decide against using flexible-aperture photometry from SExtractor because of the differently sized apertures used for the same galaxy across the IRAC channels. Instead, we use a constant 15″ diameter aperture (6 kpc at Coma's mean redshift) and apply aperture corrections to the extended objects as detailed in the IRAC Instrument Handbook.

Not surprisingly, we find that an overwhelming majority of Coma galaxies occupy the "passive cloud" in IRAC color space and well below the AGN wedge. The dispersion in the [5.8]−[8.0] color is likely due to PAH features from star formation at 6.2μm and 7.7μm being detected in IRAC's 8.0μm bandpass; note that Coma's proximity means we detect even the faintest members. There is one member with a significantly redder [3.6]−[4.5] color that is a disk galaxy viewed at an intermediate angle, but it is not an IR-AGN from the [89] criteria and is not classified as an optical AGN in the recent survey of Coma by [65].

3.2.2 Abell 1689

Spectroscopically confirmed members and their photometry are from [30]. The scatter in [5.8]−[8.0] color among members can be attributed to PAH features at 3.3, 6.2 and 7.7μm in dusty star forming galaxies where the latter two features both shift into the 8.0μm channel. However, the 3.3μm PAH feature shifts to the boundary between channels 1 & 2. We find one candidate IR-AGN for this low redshift cluster that has also been classified as a Seyfert 1 AGN based on optical spectroscopy [30]. This prior study of Abell 1689 included mid-IR measurements from ISOCAM and the authors concluded that dusty star formation in this cluster is responsible for the vast majority of the observed mid-IR emission. Our results support this conclusion as we find no other members with infrared AGN signatures.

3.2.3 MS 1358+62

Photometry and spectroscopic information of MS 1358 members is from [38]. At $z = 0.33$, the 3.3 and 6.2μm PAH features shift into IRAC channels 2 & 4 respectively and colors along both axes are redder. This explains the dispersion seen in Figure 3.2 for late-type galaxies that are likely to be star forming. The spectroscopic study of this cluster by [38] revealed a number of emission line galaxies (ELGs). Not surprisingly, nearly all of the galaxies that depart from the "passive cloud" are also ELGs. Of the galaxies in this cluster, we find one candidate AGN that is hosted by a late-type spiral. [68] find no X-ray AGN in this cluster with L(2-8 keV) $\geq 10^{43}$ ergs s^{-1}. The one galaxy that we select as an AGN is detected as an ELG located roughly 860 kpc from the cluster center.

3.2.4 CL 0024+17

Spectroscopy and photometry for CL 0024 is from [74]. Star-forming members with PAH emission are subject to the same effects as described for MS 1358 and thus produce a similar scatter in mid-IR color-color space. The scatter here makes it difficult to discern the nature of the galaxies that are found near the boundary of the wedge. We do find two galaxies in the AGN-wedge (one appears to be sitting on the boundary). For the galaxy on the boundary, it is probable that star formation is producing its colors, though it is not ruled out as hosting an IR-weak AGN. The other candidate AGN we find shows colors consistent with a power-law spectrum placing it well inside the IRAC wedge. [101] have conducted an X-ray observation of this cluster locating a handful of point sources at $L_X > 10^{42}$ ergs s^{-1}. However, none of the X-ray point sources overlap with any cluster galaxies from the spectroscopic catalog, i.e. these X-ray sources are in the field.

CL 0024 is known to have numerous substructures as traced by three techniques: weak-lensing map [58], X-ray shock fronts [101] and a Dressler-Shectman test [74][29].

This implies that many galaxies are in groups that have been recently accreted (or are in the process) into the main cluster. Furthermore, the redshift distribution of galaxies shows a bimodality that suggests a recent merger along the line of sight with a large galaxy group [19][20]. The one candidate AGN that is well inside the wedge has two close neighbors (confirmed spectroscopically) and is located ∼0.84 Mpc from the cluster center (see Figure 3.3). Redshifts of these galaxies are consistent with the main cluster. The candidate IR-AGN that we find near the edge of the IRAC-wedge is also within the main cluster; it is closer to the cluster core (∼340 kpc) but is >80 kpc from the nearest neighboring galaxy.

3.2.5 MS 0451-03

Spectroscopy and photometry for MS 0451 are also from [74]. At $z = 0.54$, the 6.2μm PAH feature shifts nearly outside the IRAC window. This reduces the scatter in mid-IR color due to star formation for members. X-ray data have shown that the distribution of the cluster ICM is predominantly elliptical [26], and the redshift distribution of cluster galaxies is broadly Gaussian [74]. This indicates that MS 0451 is predominantly virialized with no substantial infalling galaxies. We detect no IR-AGN and no cluster galaxies are detected as X-ray sources based on a *Chandra* survey [72], further indicating a lack of strong nuclear activity in MS 0451.

3.2.6 MS 2053-04

Spectroscopic and photometric information of galaxies in this cluster come from [92]. Detailed spectroscopic and gravitational lensing studies of MS 2053-04 [98][92] show that it is a merger of two structures with 113 and 36 confirmed members respectively. Galaxies in the smaller structure (2053-B) have similar properties to field galaxies not associated with the cluster. This, coupled with the high fraction of star forming members (∼44%), suggests that MS 2053 has yet to completely virialize.

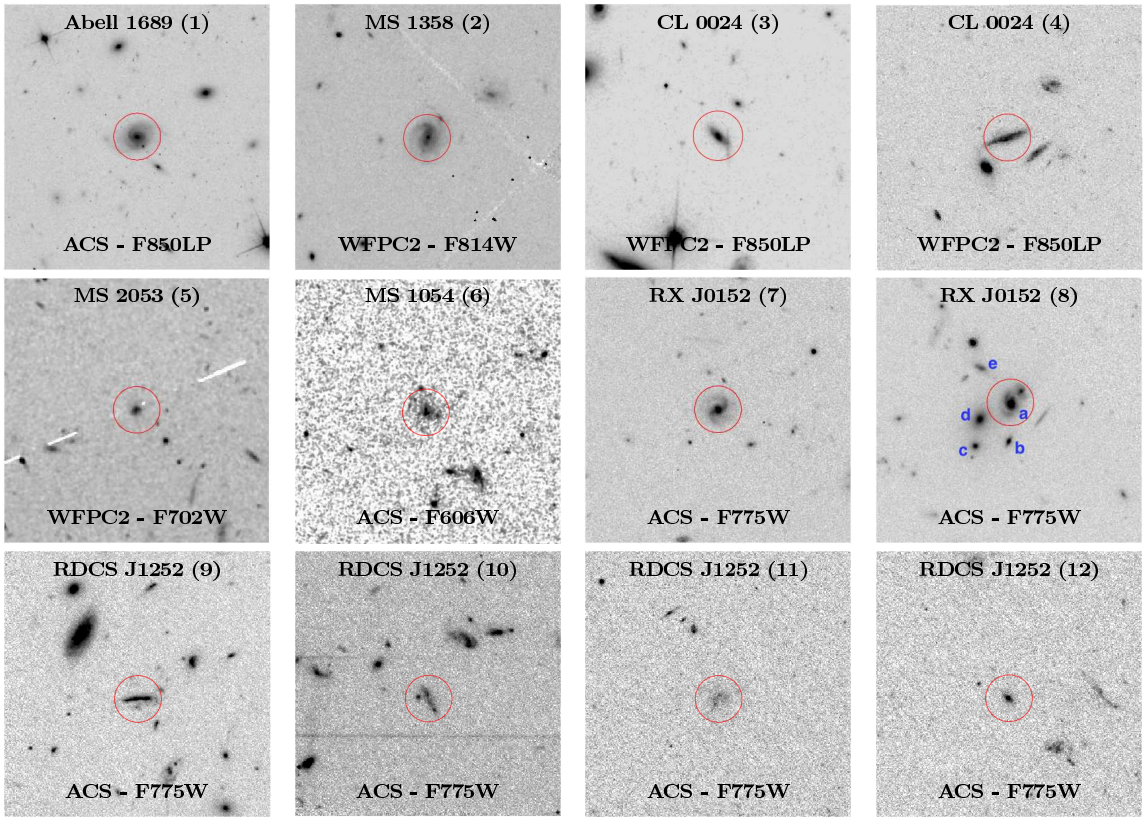

Fig. 3.3. Thumbnails of our sample of infrared-selected AGN; images are from the *Hubble Space Telescope*. Numbers in parentheses correspond to the ID from Table 4.1. All images are ∼150×150 kpc and are oriented North-up, East-left. Red circles correspond to the aperture of constant size ($r \approx 12.6$ kpc) used to perform photometry on the IRAC images. See §3.2.8 for an explanation of the labels in panel 8.

Observations with *Spitzer*/MIPS also find that a fairly high fraction ($\sim$18%) of cluster members are detected at 24μm [85], and the large population of star forming members clearly separates from the passive members in mid-IR color. Given the high level of activity in MS 2053, it is surprising then that it only has one weak IR-AGN candidate. Using archival *Chandra* data, [32] find five X-ray sources at the redshift of MS 2053 with $L_{X,H} > 10^{42}$ ergs/s. However, three are not classified as cluster members due to their distances from the cluster center ($r > r_{200}$) and another is the BCG which is thought to be contaminated by X-ray emission from the ICM. This leaves only one cluster X-ray AGN which has a [3.6]$-$[4.5] color that is bluer than the IR-AGN selection region (Figure 3.2).

3.2.7 MS 1054-03

Spectroscopically confirmed members and photometry are taken from [94]. One cluster X-ray source was not included in the photometric catalog, but optical and X-ray data for this galaxy are available from [67]. Weak-lensing and X-ray analyses of MS 1054 show a clumpy nature to the dark matter and ICM profiles [56]. The presence of such substructure indicates that the cluster experienced a merger and has yet to fully virialized.

Earlier studies of MS 1054 reveal that it contains two members hosting X-ray AGN [57] and 8 radio sources that can be powered by AGN or star formation [9]. We find only one infrared AGN at a distance $\gtrsim$1 Mpc from the cluster center that is also detected as both an X-ray and radio source. The second X-ray source lies near the edge of the IRAC footprints and is not detected at 5.8μm. Though this does not allow it to be identified as IR-AGN, it is not ruled out based on its [3.6]$-$[4.5] color (Figure 3.2).

3.2.8 RX J0152-13

Spectroscopic membership of cluster galaxies is from [22] and photometry from [11]. This cluster shows signs of having gone through a large-scale merger event recently as indicated by its X-ray emission, luminosity distribution and weak-lensing profile [55].

We detect two IR-AGN in this cluster, both of which are classified as X-ray QSOs [67]; no other cluster galaxies are detected as X-ray sources. One of the IR+X-ray AGN is about 800 kpc from the cluster core while the second appears to be in a merging system. The latter detection is associated with five cluster galaxies within a projected radius of 30 kpc (Figure 3.3, neighboring cluster galaxies are labeled). Due to their proximity and the IRAC PSF, these galaxies are blended into one mid-IR source where galaxy a is the closest ($\sim$0.7") to the centroid of the mid-IR emission. Redshifts in this quintet are 0.867, 0.864, 0.834, 0.832 and 0.836 for galaxies a, b, c, d and e respectively. Based on these redshifts, recessional velocities ($w.r.t.$ to galaxy c) are 3743, 3408, 0, -231 and 231 km/s for galaxies a, b, c, d and e respectively. Since galaxies a & b have velocities within 400 km/s and galaxies c, d & e have velocities within 500 km/s (typical of galaxy groups) we suspect a & b are a bound system and c, d & e are another bound system. Note, however, that a chance alignment of two groups such as this is $\sim$0.1% likely to occur at random assuming a spherical cluster geometry with $R \approx 1$ Mpc. Of course, due to the complex morphology and substructure in RX J0152 [55] this probability may increase.

3.2.9 RDCS J1252-29

At $z = 1.24$, RDCS 1252 is the most distant cluster in our sample yet has a virial mass similar to those of the lower redshift clusters as well as other properties [83]. Close inspection of the ICM in the cluster core reveals the presence of a shock front, signaling a recent merger with a cluster sub-clump. A detailed spectroscopic

follow-up [23] verifies a merger of two groups that have yet to viralize, and weak lensing shows that the centroid of the dark matter mass profile is offset from the optical/X-ray centroid by ∼8" [63]. Yet despite its young dynamical age, RDCS 1252 already has a population of luminous early-type galaxies that show little sign of ongoing star formation.

At this redshift, emission from stellar populations begins to encroach into the IRAC window. This effect can be seen in Figure 3.2 as an upward shift in the the "passive cloud" relative to the lower-z clusters. This unfortunately brings the "passive cloud" closer to the AGN-wedge, possibly introducing contamination. Of the twenty nine RDCS 1252 members shown in Figure 3.2, four are inside the AGN-wedge, of which one has been previously identified as an X-ray AGN [67][23]. Three of the four candidate IR-AGN are hosted by morphologically irregular galaxies (Figure 3.3) that are likely to be gravitationally disrupted because of the large-scale cluster merger or by galaxy-galaxy mergers (*HST* images from [10] and [23]).

4. DISCUSSION

4.1 Cluster IR-AGN Properties

Recent studies of field galaxies find that infrared-selected AGN share similar properties [48][44]: their host galaxies typically have late-type morphologies and tend to have blue optical colors. The properties of our 12 cluster IR-AGN agree with these earlier studies. We find the majority of our IR-selected AGN (10/12) are in late-type galaxies (Table 4.1) that are blue (Fig. 4.1) and so have recent/ongoing star formation. The remaining two cluster IR-AGN are hosted by S0 galaxies that lie on/near the IR-AGN boundary (Fig. 3.2) and these members are consistent with being spiral galaxies transitioning to early-type systems in the cluster environment [28][74].

It is worth noting that optical light from host galaxies may be contaminated by emission from an AGN, thus their colors could be biased bluewards. Our bluest AGN host, for example, is likely contaminated by the central engine since it is such a strong outlier. Figure 3.3 shows ACS & WFPC-2 images of our IR-selected AGN, nearly all at rest-frame blue wavelengths. Upon careful visual inspection we find that the majority of these galaxies have extended morphologies and are not strongly dominated by a central point source. Furthermore, [48] calculated color contamination to be $\lesssim 0.3$ mag in ${}^{0.1}(u-r)$[1]. When considering that the optical filters we use $(B-V)$ are closer together in wavelength space and that AGN generally contribute more flux at bluer wavelengths, we expect color contamination in our sample to be less than what [48] find. Therefore, although point source contamination may be impacting some of our sample, we conclude that color contamination of our IR-AGN hosts is not significant enough to bias our results.

We find that a third (4/12) of our cluster IR-AGN are also known X-ray sources [67][57], a fraction that is nominally consistent with results from the AGN and Galaxy

[1]This color is computed by blueshifting the SDSS u & r filters by $z = 0.1$

Table 4.1
IRAC-Selected Cluster AGN

ID	Cluster	RA (J2000)	Dec (J2000)	z [a]	R_{proj} [b]	$M_{3.6}$ [c]	HR[d]	$\log(L_X)$[e]	Morphology[f]
1	Abell 1689	13 11 35.5	−01 20 12.8	0.2000 (1)	0.30	-21.66±0.04	. . .	. . .	Sc
2	MS 1358	13 59 24.0	+62 31 08.0	0.3236 (2)	0.86	-21.64±0.03	. . .	. . .	Sc
3	CL 0024	00 26 40.0	+17 09 41.8	0.3955 (3)	0.33	-21.36±0.05	. . .	. . .	Sa+b
4	CL 0024	00 26 33.7	+17 12 19.8	0.3964 (3)	0.84	-21.64±0.05	. . .	. . .	Sc+d
5	MS 2053	20 56 21.0	−04 37 22.8	0.5763 (4)	0.19	-21.48±0.10	. . .	. . .	S0/a
6	MS 1054	10 57 02.7	−03 39 43.6	0.8319 (5)	1.02	-24.12±0.07	0.03±0.18	43.23	Irr
7	RX J0152	01 52 43.8	−13 59 01.3	0.8201 (5)	0.78	-23.61±0.08	-0.62±0.05	44.18	Sb
8	RX J0152	01 52 39.8	−13 57 40.7	0.8300 (5)	0.48	-24.88±0.07	-0.09±0.07	44.52	merger
9	RDCS 1252	12 52 55.6	−29 27 09.7	1.2274 (6)	0.15	-21.85±0.12	. . .	. . .	Irr
10	RDCS 1252	12 52 57.4	−29 27 32.0	1.2322 (6)	0.35	-22.28±0.12	. . .	. . .	Irr
11	RDCS 1252	12 52 49.8	−29 27 54.7	1.2382 (6)	0.59	-22.95±0.12	0.20±0.31	43.15	Irr
12	RDCS 1252	12 52 49.7	−29 28 03.7	1.2382 (6)	0.65	-22.61±0.12	. . .	. . .	S0

[a] Spectroscopic redshift: (1) [30]; (2) [38]; (3) [74]; (4) [92]; (5) [51]; (6) [23].
[b] Projected distance from the cluster center in Mpc.
[c] Rest-frame 3.6μm absolute magnitude.
[d] X-ray hardness ratio from [67] for AGN with X-ray detections.
[e] Hard X-ray (2-10 keV) luminosity in ergs s^{-1} from Martel et al. 2007.
[f] Morphology references: [70](Coma), [30](Abell 1689), [34](MS 1358), [74](CL 0024), [75](MS 0451), [93](MS 2053), [11](MS 1054), [11](RX J0152) and [23](RDCS J1252)

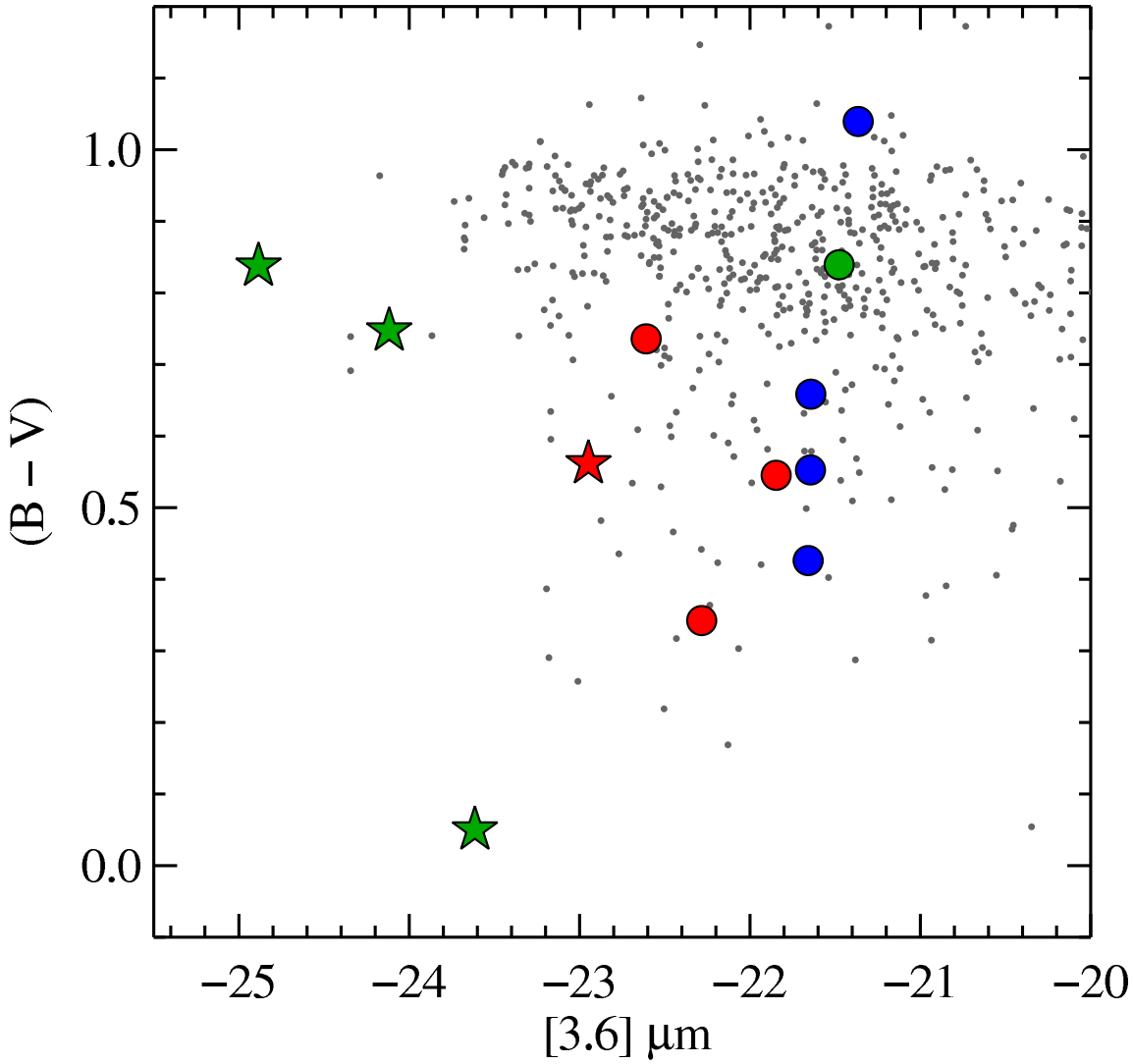

Fig. 4.1. Rest-frame color-magnitude relation (optical color vs. 3.6μm absolute magnitude). Host galaxies of IR-AGN tend to have blue optical colors, thus these IR-AGN hosts have recent/ongoing star formation. Also, the four most luminous cluster IR-AGN are also X-ray sources.

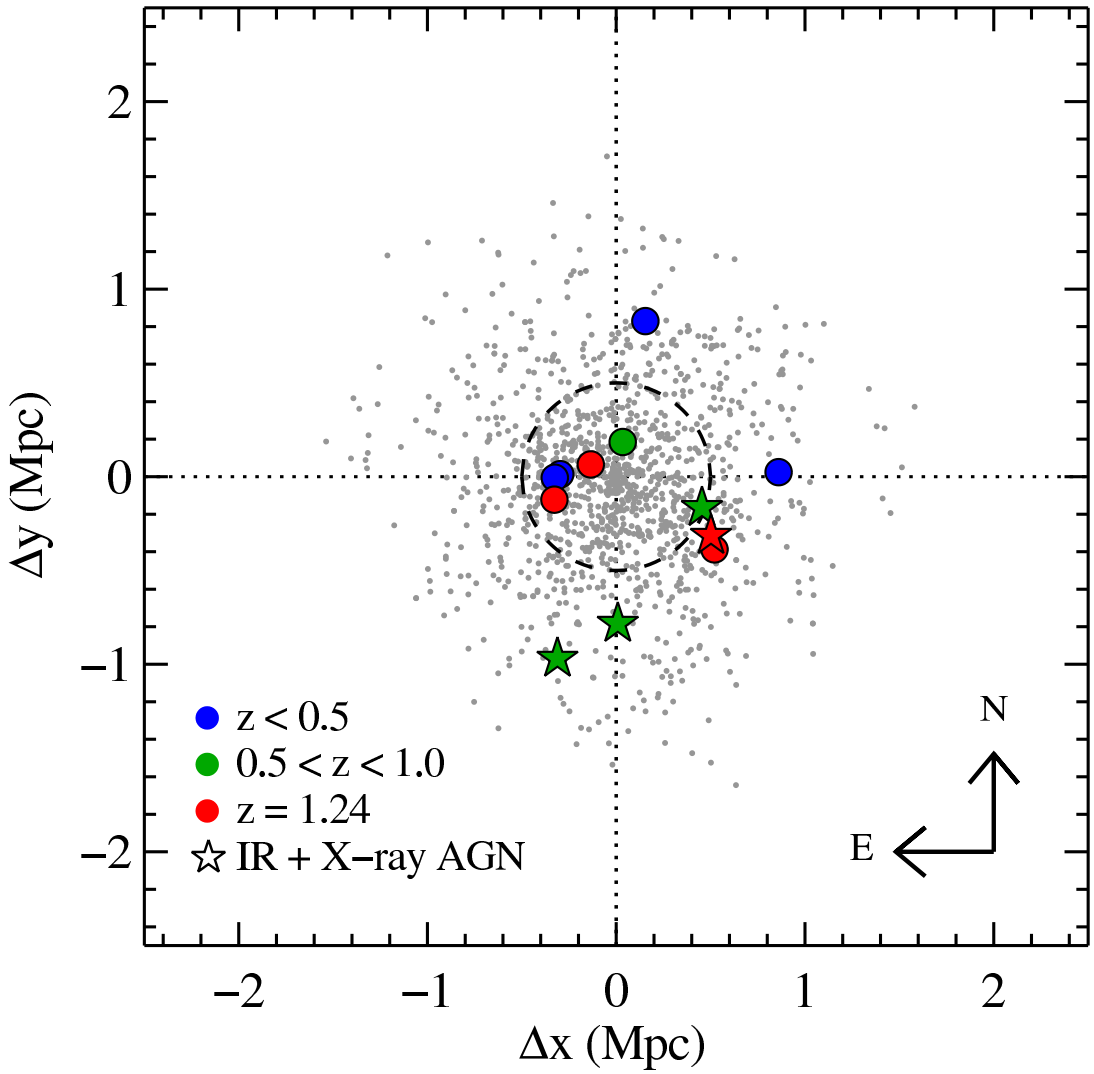

Fig. 4.2. Combined sky-plot for each cluster showing the projected locations of galaxies with respect to their cluster centers; symbols are the same as in figure 4.1. IRAC-selected AGN are shown as circles (or stars for X-ray sources) and the dashed circle corresponds to a physical radius of 0.5 Mpc. Colors correspond to three bins is redshift, $z < 0.5$ (blue), $0.5 < z < 1.0$ (green) and $z = 1.24$ (red). A Kolmogorov-Smirnov test shows that the radial distribution of the IR-AGN is >99% likely to come from the same parent population as the normal cluster galaxies (gray points).

Evolution Survey (AGES) where $\sim$ 50% of IR-AGN are also X-ray sources [48]. However, it is worth mentioning here that X-ray flux limits are not the same among these studies, and so agreement on this ratio is not necessarily implied. The X-ray

sources are also the four most luminous 3.6μm IR-AGN (rest-frame; Figure 4.1); however, note that the most luminous cluster IR+X-ray AGN is the blended source in RX J0152 (see §3.2.8).

Figure 4.2 shows the projected distances of the 12 IR-AGN relative to confirmed members in all nine galaxy clusters. We find the radial distribution of the IR-AGN is drawn from the same parent population as the cluster galaxies with $> 99\%$ confidence using a Kolmogorov-Smirnov test. However, the four IR+X-ray AGN are all outside the cluster cores at $R_{proj} \gtrsim 0.5$ Mpc. This result is consistent with [32] and [3] who find that X-ray sources in galaxy clusters are not strongly centrally concentrated. Our observations may suggest that IR+X-ray AGN represent a different population than IR-only AGN; however, we are limited by the size of our sample and so cannot further postulate on the uniqueness of these AGN based on their spatial distribution and 3.6μm luminosities.

4.2 Infrared-AGN Fractions

To measure the fraction of IR-AGN in our cluster sample and test for evolution, we separate our sample into three redshift bins: low redshift (< 0.5), intermediate redshift ($0.5 < z < 1.0$), and a high redshift point at $z = 1.24$ (RDCS 1252) containing 543, 377 and 29 IRAC detected members respectively. To ensure robustness, we consider two different galaxy samples selected optically and in the mid-IR. We also take into account the varying spatial coverage of the IRAC mosaics and set the maximum field of view with the Coma cluster where the IRAC footprint only includes galaxies within $R_{proj} \sim 760$ kpc of the cluster center. In the higher redshift clusters, we therefore exclude members that are at $R_{proj} > 760$ kpc from their cluster center.

Our first cluster galaxy sample is composed of optically-selected members brighter than $V = -21.5$ (this corresponds to where the V-magnitude distribution turns over for RDCS 1252, our most distant cluster); this yields 118, 141 and 22 galaxies in our three redshift bins. Note we do not to correct for passive evolution given that

the host galaxies of the IR-AGN tend to have blue optical colors, i.e. are likely star forming systems. The IR-AGN fraction for this optically-selected sample is $\sim 1\%$ for both redshift bins at $z < 1$ and is only measurably non-zero at $z = 1.24$ with $f_{\rm IR-AGN}$=$18.2^{+14}_{-8.7}\%$ (Table 4.2; Fig. 4.3). All errors in $f_{\rm IR-AGN}$ are asymmetric 1σ Poisson uncertainties as determined by [43] for small number samples.

Our second cluster galaxy sample is composed of members selected based on rest-frame 3.6μm luminosity. Because of the evolution of the 3.6μm luminosity function is well-characterized by passively evolving galaxies that formed at $z > 1.5$ [76], this luminosity selection is effectively a stellar mass cut. To isolate comparable samples of cluster members over our redshift range, we combine values of $M^{\star}(z)$[3.6μm] (the characteristic turning point in the Schechter luminosity function [88]) from [76] with the 80% limiting magnitude for our most distant cluster and thus select members brighter than rest-frame ($\rm M^{*}_{3.6}(z)$[3.6μm] + 0.5). We find that the cluster IR-AGN fraction is again uniformly $\sim 1\%$ at $z < 1$ and only measurably non-zero at $z = 1.24$ with $f_{\rm IR-AGN}$=$13.6^{+13}_{-7.4}\%$ (RDCS 1252; Table 4.2; Fig. 4.3).

Thus far we have included all cluster galaxies regardless of morphology in determining $f_{\rm IR-AGN}$, but this may introduce a bias given that: 1) our cluster IR-AGN are predominantly hosted by late-type galaxies and 2) the morphological mix in clusters evolves with redshift [28][36][78][16]. In Fig. 4.4 we now exclude all morphologically classified E/S0 members and measure a higher $f_{\rm IR-AGN}$ at all redshifts (Table 4.2). However, $f_{\rm IR-AGN}$ remains $\lesssim 5\%$ at $z < 1$ in both of our selected galaxy samples. Only in the most distant cluster (RDCS 1252) does $f_{\rm IR-AGN}$ for late-type[1] members increase to $\sim 70\%$.

Although the number of cluster IR-AGN is small, we stress that our analysis is based on a sample of $\sim$ 1500 spectroscopically confirmed cluster galaxies at $0 < z < 1.3$, thus we place a strong upper limit on the IR-AGN fraction of $\lesssim 3\%$ for all members in massive clusters at $z < 1$. One caveat to consider is that while

[1]Here we mean all members except for E/S0s.

Table 4.2
IR-AGN Fractions

Selection[a]	z-bin	N_{AGN}	N_{tot}	$f_{\mathrm{IR-AGN}}$[b]
All Cluster Members	$(z < 0.5)$	1	291	$0.3^{+0.8}_{-0.3}$ %
$M_{3.6} < M^*_{3.6}$+0.5 mag	$(0.5 < z < 1.0)$	1	143	$0.7^{+1.6}_{-0.6}$ %
	$z = 1.24$	3	22	$13.6^{+13}_{-7.4}$ %
All Cluster Members	$(z < 0.5)$	1	118	$0.8^{+1.9}_{-0.7}$ %
$V_{AB} < -21.5$ mag	$(0.5 < z < 1.0)$	1	141	$0.7^{+1.6}_{-0.6}$ %
	$z = 1.24$	4	22	$18.2^{+14}_{-8.7}$ %
Late-Types Only	$(z < 0.5)$	1	43	$2.3^{+5.3}_{-1.9}$ %
$M_{3.6} < M^*_{3.6}$+0.5 mag	$(0.5 < z < 1.0)$	1	21	$4.7^{+11}_{-3.9}$ %
	$z = 1.24$	2	3	67^{+33}_{-43} %
Late-Types Only	$(z < 0.5)$	1	24	$4.1^{+9.6}_{-3.4}$ %
$V_{AB} < -21.5$ mag	$(0.5 < z < 1.0)$	1	26	$3.8^{+8.8}_{-3.2}$ %
	$z = 1.24$	3	4	75^{+25}_{-41} %

[a] Members are selected using a luminosity limit in rest-frame 3.6μm or rest-frame V_{AB}.
[b] Uncertainties in $f_{\mathrm{IR-AGN}}$ represent 1σ Poisson errors determined from [43].

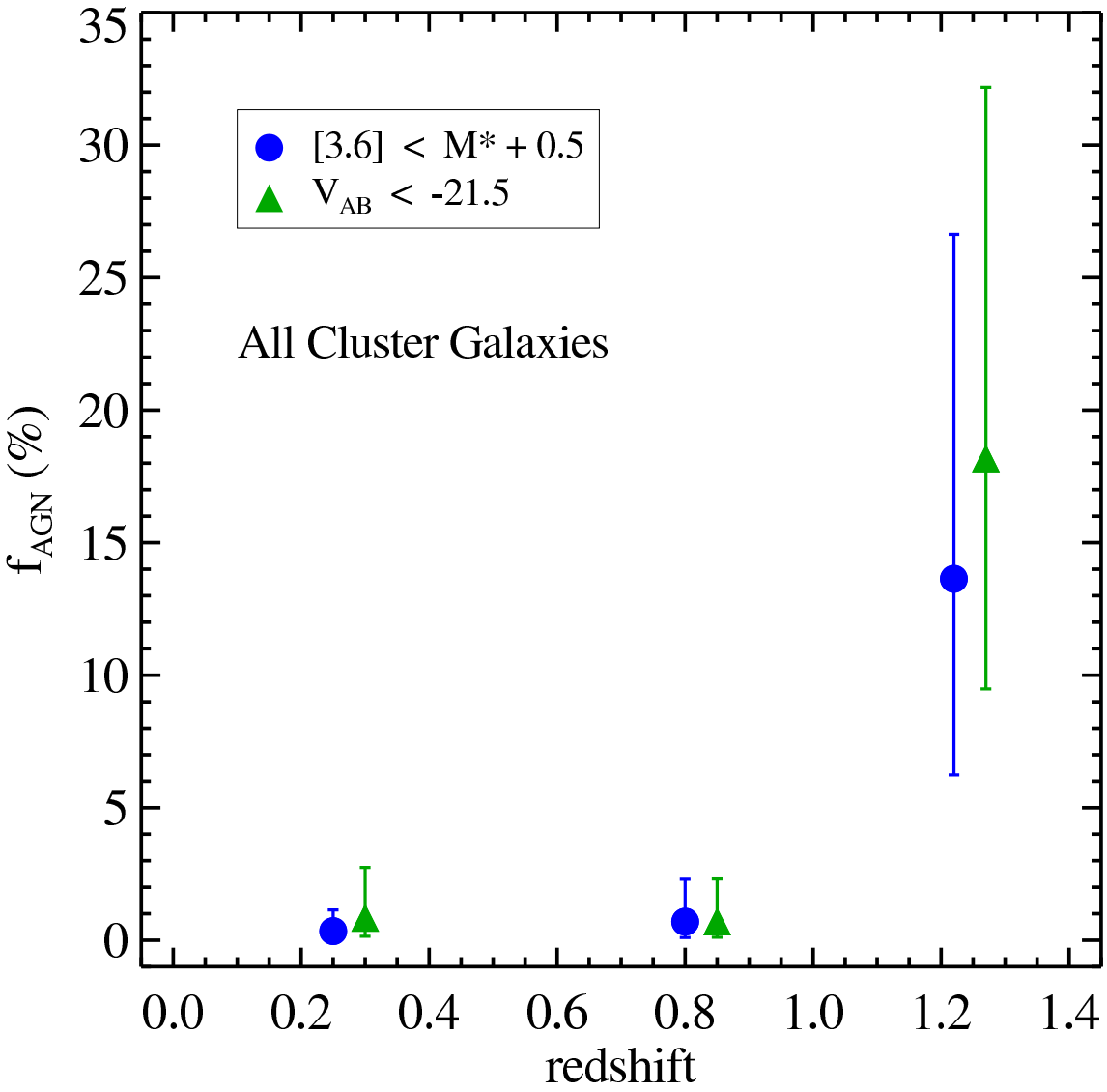

Fig. 4.3. Cluster IR-AGN fraction as a function of redshift for optically selected members brighter than $V_{AB} = -21.5$ mag (green triangles) and mid-IR selected members brighter than $(M^*_{3.6} + 0.5)$ (blue circles). We consider three redshift bins: low redshift ($z < 0.5$), intermediate redshift ($0.5 < z < 1.0$), and a high redshift point at $z = 1.24$ (RDCS 1252) that contain 543, 377, and 29 IRAC-detected members respectively. The IR-AGN fraction is uniformly $\lesssim 3\%$ at $z < 1$ and only measurably higher in RDCS 1252 at $z = 1.24$. Error bars represent 1σ Poisson uncertainties derived using statistics from [43].

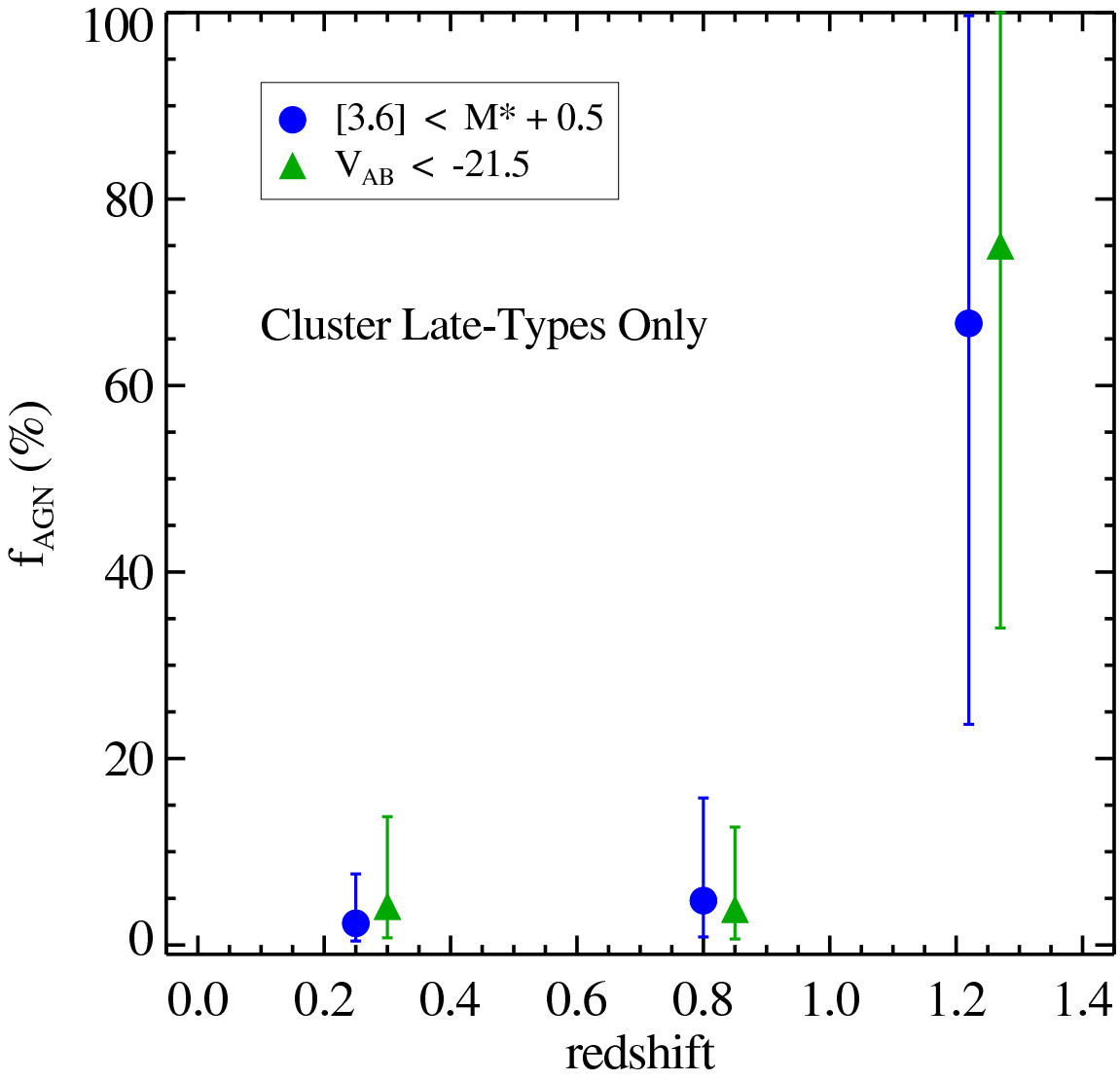

Fig. 4.4. Same as Fig. 4.3 but only considering late-type galaxies (i.e. excluding E/S0 galaxies). The IR-AGN fraction remains $\lesssim 5\%$ at $z < 1$ and is higher only at $z = 1.24$.

the IR color selection does identify $\sim 90\%$ of broad-line AGN, it misses $\sim 60\%$ of narrow-line AGN [89]and so we may be underestimating $f_{\mathrm{IR-AGN}}$. However, strongly starbursting galaxies may also contaminate our IR-AGN sample (up to $\sim 50\%$ [27]),

and accounting for these actually decreases the IR-AGN fraction. Addressing these two competing effects is beyond the scope of our current analysis.

The low IR-AGN fraction of $\sim 1\%$ in our massive clusters at $z < 1$ is consistent with [68] who estimate an X-ray AGN fraction of $0.13 - 1.00\%$ in clusters at $\bar{z} \sim 0.2$ to $\bar{z} \sim 0.7$ and with [48] who find the IR-AGN fraction in AGES is comparable to the X-ray AGN fraction at $0.25 < z < 0.8$. However, we cannot say for certain that there is strong evolution in the cluster IR-AGN fraction with redshift given our small numbers. This is in contrast to the observed increase in the fraction of (dusty) star forming members in these same clusters [85], thus the bulk of their 24μm flux is due to star formation and not AGN. Our single galaxy cluster at $z > 1$ does suggest that IR-AGN have a more prominent role at this epoch, but we recognize that 1) RDCS 1252 may be unusually active and 2) the IRAC color selection starts to suffer contamination from passive galaxies at these redshifts. Given their rarity, a larger survey of IR-AGN in massive galaxy clusters, particularly at $z > 1$, is needed to robustly identify any evolution in IR-AGN with redshift.

Another interesting comparison we can study is the variation in $f_{\mathrm{IR-AGN}}$ with environment. Using magnitude cuts similar to our $V \leq -21.5$ limit, the $f_{\mathrm{IR-AGN}}$ in the Boötes field sample from the AGES ($0.25 < z < 0.8$) is $\sim$2% (R. Hickox, private communication). This is well within our upper 1σ uncertainty (Table 4.2) at similar redshifts, thus there is no clear variation in $f_{\mathrm{IR-AGN}}$ based on local density. The possibility of AGN playing a more influential role at $z > 1$ still remains.

5. CONCLUSIONS

We present the first census of mid-infrared selected active galactic nuclei (IR-AGN) in massive galaxy clusters ($M_{\rm vir} \gtrsim 5 \times 10^{14} M_{\odot}$) at $0 < z < 1.3$ by combining archival *Spitzer*/IRAC imaging with extensive optical spectroscopic catalogs (public and private) and deep optical photometry of $\sim$ 1500 confirmed members in nine clusters. Our clusters are selected to be the most massive well-studied systems currently known. Using the four IRAC channels (3.6, 4.5, 5.8 and 8.0μm) and established mid-IR color selection techniques [89][61], we identify 949 members that are detected ($> 3\sigma$) in at least three of the four IRAC channels and isolate 12 that host dust-enshrouded AGN. Similar to IR-selected AGN in recent field studies [48][44], the host cluster galaxies tend to be late-type members with blue optical colors that indicate recent/ongoing star formation. The IR-AGN have the same radial distribution as the cluster members, but the four most IR-luminous AGN lie outside of their cluster cores ($R_{proj} > 0.5$ Mpc) and are also known X-ray sources. This suggests that very bright IR+X-ray AGN are not centrally concentrated in their clusters, consistent with the results for bright X-ray sources by [68]. Our results suggest that IR+X-ray AGN may not be the same population as the IR-only AGN, but we are too limited by our sample to make any assertion.

To measure the fraction of IR-AGN and test for evolution, we compare two complete samples of cluster galaxies: 1) an optically-selected sample with members brighter than $V_{\rm AB} = -21.5$ (rest-frame) and 2) a mid-IR selected sample with members brighter than ($M^{\star}(z)[3.6\mu{\rm m}] + 0.5$) [76] that is essentially a stellar mass cut. For the eight galaxy clusters at $z < 1$, we place a strong upper limit of $\lesssim 3\%$ on the fraction of IR-AGN for both cluster samples. Because IR-AGN tend to be hosted by late-type galaxies and the morphological mix in clusters evolves [28][78], we also consider only late-type members and find that the fraction with IR-AGN is $\lesssim 5\%$ for both samples. These low IR-AGN fractions are surprising given that the

fraction of (dusty) star formation in these same clusters increases by about a factor of four at $0 < z < 1$ [85][4]. However, an IR-AGN fraction of $\sim 1\%$ is consistent with the low fraction of X-ray AGN in galaxy clusters ($\leq 1\%$, [68]) and the relative populations of X-ray vs. IR AGN [48].

In contrast, our single galaxy cluster at $z = 1.24$ (RDCS 1252) has a measurably higher IR-AGN fraction of $\sim 15\%$ (all galaxy types) and $\sim 70\%$ (late-types only). However, RDCS 1252 may simply be an unusually active cluster. Also, the IR color selection starts to suffer stronger contamination from non-AGN members at $z > 1.2$.

We also compare our $f_{\rm IR-AGN}$ measurements in dense clusters at $z < 1$ to that of the Boötes field from the AGES, which probes sparser galactic environments over a similar range in redshift ($0.25 < z < 0.8$). Using optical magnitude cuts similar to this study, $f_{\rm IR-AGN}$ is measured to be $\sim$2% in the field (R. Hickox, private communication). Consequently, we do not see a statistically significant variation in $f_{\rm IR-AGN}$ here that would be caused by local galaxy density. However, the question still remains as to whether or not IR-AGN have a more profound impact at $z > 1$.

We note that while the IR color selection successfully identifies $\sim 90\%$ of broad-line AGN, it does miss $\sim 60\%$ of narrow-line AGN [89] and so $f_{\rm IR-AGN}$ is undoubtedly incomplete, i.e. underestimated. On the other hand, contamination may arise from star forming galaxies falsely identified as IR-AGN; thus we may also be overestimating $f_{\rm IR-AGN}$. Such contamination can be as high as 20–50% [27][48] and is more influential at low luminosities. For simplicity, we ignore these two competing effects because they are beyond the scope of our analysis and do not change our general conclusions.

Taken as a whole, our results show that IR-AGN and star formation are not strongly correlated at $z < 1$ because the IR-AGN fraction is uniformly very low ($\sim 1\%$) at $z < 1$ whereas several of these clusters have star forming fractions of $\gtrsim 20\%$ [85]. We do find a hint of evolution in the IR-AGN fraction at $z \sim 1.2$, but only with a more extensive mid-IR survey of galaxy clusters, particularly at

$z > 1$, can we confirm this intriguing result. A study with equally deep spectroscopic coverage across this wide redshift range is also needed to robustly measure $f_{\rm IR-AGN}$ and test for evolution as a function of environment. While *Spitzer*/IRAC is no longer available, such studies should be possible with the upcoming public survey by the *Wide-field Infrared Survey Explorer* (WISE).

REFERENCES

[1] Andreani P., Cristiani S., Grazian A., La Franca F., & Goldschmidt P. 2003, AJ, 125, 444

[2] Ashby M., Stern D., Brodwin M., Griffith R., Eisenhardt P., et al. 2009, ApJ, 701, 428

[3] Atlee D. W., Martini P., Assef R. J., Kelson D. D., & Mulchaey J. S. 2011, ApJ, 729, 22

[4] Bai L., Rasmussen J., Mulchaey J. S., Dariush A., Raychaudhury S., & Ponman T. J. 2010, ApJ, 713, 637

[5] Bardeau S., Soucail G., Kneib J., Czoske O., Ebeling H., Hudelot P., Smail I., & Smith G. P. 2007, A&A, 470, 449

[6] Barmby P., Alonso-Herrero A., Donley J. L., Egami E., Fazio, G. G., et al. 2006, ApJ, 642, 126

[7] Barmby P., Huang J., Ashby M. L. N., Eisenhardt P. R. M., Fazio G. G., Willner S. P., & Wright E. L. 2008, ApJS, 177, 431

[8] Bertin E., & Arnouts S. 1996, A&AS, 117, 393

[9] Best P. N., van Dokkum P. G., Franx M., & Röttgering H. J. A. 2002, MNRAS, 330, 17

[10] Blakeslee J. P., Franx M., and Postman M., and Rosati P., and Holden B. P., et al. 2003, ApJ, 596, L143

[11] Blakeslee J. P., Holden B. P., Franx M., Rosati P., Bouwens R. J., et al. 2006, ApJ, 644, 30

[12] Blanton M. R., & Roweis S. 2007, AJ, 133, 734

[14] Bower R. G., Lucey J. R., & Ellis R. S. 1992, MNRAS, 254, 589

[13] Bower R. G., Benson A. J., Malbon R., Helly J. C., Frenk C. S., Baugh C. M., Cole S., & Lacey C. G. 2006, MNRAS, 370, 645

[15] Bower R. G., McCarthy I. G., & Benson A. J. 2008, MNRAS, 390, 1399

[16] Capak P., Abraham R. G., Ellis R. S., Mobasher B., Scoville N., Sheth K., & Koekemoer A. 2007, ApJS, 172, 284

[17] Chung S. M., Gonzalez A. H., Clowe D., Markevitch M., & Zaritsky D. 2010, ApJ, 725, 1536

[18] Croton D. J., Springel V., White S. D. M., De Lucia G., Frenk, et al. 2006, MNRAS, 365, 11

[19] Czoske O., Kneib J., Soucail G., Bridges T. J., Mellier Y., & Cuillandre J. 2001, A&A, 372, 391

[20] Czoske O., Moore B., Kneib J., & Soucail G. 2002, A&A, 386, 31

[21] De Lucia G., Poggianti B. M., Aragón-Salamanca A., White S. D. M., Zaritsky D., et al. 2007, MNRAS, 374, 809

[23] Demarco R., Rosati P., Lidman C., Homeier N. L., Scannapieco E., et al. 2005, A&A, 432, 381

[22] Demarco R., Rosati P., Lidman C., Girardi M., Nonino M., et al. 2007, ApJ, 663, 164

[24] Devriendt J. E. G., Guiderdoni B., & Sadat R. 1999, A&A, 350, 381

[26] Donahue M., Voit G. M., Scharf C. A., Gioia I. M., Mullis C. R., Hughes J. P., & Stocke J. T. 1999, ApJ, 527, 525

[25] Donahue M., Gaskin J. A., Patel S. K., Joy M., Clowe D., & Hughes J. P. 2003, ApJ, 598, 190

[27] Donley J. L., Rieke G. H., Pérez-González P. G., & Barro G. 2008, ApJ, 687, 111

[29] Dressler A., & Shectman S. A. 1988, AJ, 95, 985

[28] Dressler A., Oemler Jr. A., Couch W. J., Smail I., Ellis R. S., et al. 1997, ApJ, 490, 577

[30] Duc P., Poggianti B. M., Fadda D., Elbaz D., Flores H., et al. 2002, A&A, 382, 60

[31] Dye S., Taylor A. N., Thommes E. M., Meisenheimer K., Wolf C., & Peacock J. A. 2001, MNRAS, 321, 685

[32] Eastman J., Martini P., Sivakoff G., Kelson D. D., Mulchaey J. S., & Tran K. 2007, ApJ, 664, L9

[33] Elvis M., Wilkes B. J., McDowell J. C., Green R. F., Bechtold J., et al. 1994, ApJS, 95, 1

[34] Fabricant D., Franx M., & van Dokkum P. 2000, ApJ, 539, 577

[35] Farouki R., & Shapiro S. L. 1981, ApJ, 243, 32

[36] Fasano G., Poggianti B. M., Couch W. J., Bettoni D., Kjærgaard P., & Moles M. 2000, ApJ, 542, 673

[37] Fazio G. G., Hora J. L., Allen L. E., Ashby M. L. N., Barmby P., et al. 2004, ApJS, 154, 10

[38] Fisher D., Fabricant D., Franx M., & van Dokkum P. 1998, ApJ, 498, 195

[39] Fontanot F., Pasquali A., De Lucia G., van den Bosch F. C., Somerville R. S., & Kang X. 2010, ArXiv e-prints

[40] Gabor J. M., Davé R., Finlator K., & Oppenheimer B. D. 2010, MNRAS, 407, 749

[41] Galametz A., Stern D., Eisenhardt P. R. M., Brodwin M., Brown M. J. I., et al. 2009, ApJ, 694, 1309

[42] Gandhi P., Horst H., Smette A., Hönig S., Comastri A., Gilli R., Vignali C., & Duschl W. 2009, A&A, 502, 457

[43] Gehrels N. 1986, ApJ, 303, 336

[44] Griffith R. L., & Stern D. 2010, AJ, 140, 533

[45] Gunn J. E., & Gott J. R., III. 1972, ApJ, 176, 1

[46] Hart Q. N., Stocke J. T., & Hallman E. J. 2009, ApJ, 705, 854

[47] Hickox R. C., Jones C., Forman W. R., Murray S. S., Brodwin M., et al. 2007, ApJ, 671, 1365

[48] Hickox R. C., Jones C., Forman W. R., Murray S. S., Kochanek C. S., et al. 2009, ApJ, 696, 891

[49] Hilton M., Lloyd-Davies E., Stanford S. A., Stott J. P., Collins C. A., et al. 2010, ApJ, 718, 133

[50] Hogg D. W., Blanton M. R., Brinchmann J., Eisenstein D. J., Schlegel D. J., et al. 2004, ApJ, 601, L29

[51] Holden B. P., Illingworth G. D., Franx M., Blakeslee J. P., Postman M., et al. 2007, ApJ, 670, 190

[52] Hopkins P. F., & Hernquist L. 2006, ApJS, 166, 1

[53] Hopkins P. F., Hickox R., Quataert E., & Hernquist L. 2009, MNRAS, 398, 333

[54] Jee M. J., White R. L., Benítez N., Ford H. C., Blakeslee J. P., Rosati P., Demarco R., & Illingworth G. D. 2005a, ApJ, 618, 46

[55] Jee M. J., White R. L., Ford H. C., Blakeslee J. P., Illingworth G. D., Coe D. A., & Tran K. 2005b, ApJ, 634, 813

[56] Johnson O., Best P. N., & Almaini O. 2003, MNRAS, 343, 924

[57] Kneib J., Hudelot P., Ellis R. S., Treu T., Smith G. P., et al. 2003, ApJ, 598, 804

[58] Kocevski D. D., Lubin L. M., Lemaux B. C., Gal R. R., Fassnacht C. D., & Squires G. K. 2009, ApJ, 703, L33

[59] Kuraszkiewicz J. K., Wilkes B. J., Hooper E. J., McLeod K. K., Wood K., et al. 2003, ApJ, 590, 128

[60] Lacy M., Storrie-Lombardi L. J., Sajina A., Appleton P. N., Armus L., et al. 2004, ApJS, 154, 166

[61] Lagos C. D. P., Cora S. A., & Padilla N. D. 2008, MNRAS, 388, 587

[62] Lombardi M., Rosati P., Blakeslee J. P., Ettori S., Demarco R., et al. 2005, ApJ, 623, 42

[63] Lubin L. M., Gal R. R., Lemaux B. C., Kocevski D. D., & Squires G. K. 2009, AJ, 137, 4867

[64] Mahajan S., Haines C. P., & Raychaudhury S. 2010, MNRAS, 404, 1745

[65] Makovoz D., Roby T., Khan I., & Booth H. 2006, Society of Photo-Optical Instrumentation Engineers (SPIE) Conference Series, 6274

[66] Martel A. R., Menanteau F., Tozzi P., Ford H. C., & Infante L. 2007, ApJS, 168, 19

[67] Martini P., Sivakoff, G. R., & Mulchaey, J. S. 2009, Astrophys.J., 701, 66

[68] McCarthy I. G., Schaye J., Ponman T. J., Bower R. G., Booth C. M., et al. 2010, MNRAS, 406, 822

[69] Michard R., & Andreon S. 2008, A&A, 490, 923

[70] Mobasher B., Bridges T. J., Carter D., Poggianti B. M., Komiyama Y., et al. 2001, ApJS, 137, 279

[71] Molnar S. M., Hughes J. P., Donahue M., & Joy M. 2002, ApJ, 573, L91

[72] Moran S. M., Ellis R. S., Treu T., Smail I., Dressler A., Coil A. L., & Smith G. P. 2005, ApJ, 634, 977

[73] Moran S. M., Ellis R. S., Treu T., Smith G. P., Rich R. M., & Smail I. 2007a, ApJ, 671, 1503

[74] Moran S. M., Miller N., Treu T., Ellis R. S., & Smith G. P. 2007b, ApJ, 659, 1138

[75] Muzzin A., Wilson G., Lacy M., Yee H. K. C., & Stanford S. A. 2008, ApJ, 686, 966

[76] Polletta M., Tajer M., Maraschi L., Trinchieri G., Lonsdale C. J., et al. 2007, ApJ, 663, 81

[77] Postman M., Franx M., Cross N. J. G., Holden B., Ford H. C., et al. 2005, ApJ, 623, 721

[78] Puchwein E., Sijacki D., & Springel V. 2008, ApJ, 687, L53

[79] Reach W. T., Megeath S. T., Cohen M., Hora J., Carey S., et al. 2005, PASP, 117, 978

[80] Richstone D. O. 1976, ApJ, 204, 642

[81] Rines K., Geller M. J., Kurtz M. J., & Diaferio A. 2003, AJ, 126, 2152

[82] Rosati P., Tozzi P., Ettori S., Mainieri V., Demarco R., et al. 2004, AJ, 127, 230

[83] Rudnick G., von der Linden A., Pelló R., Aragón-Salamanca A., Marchesini D., et al. 2009, ApJ, 700, 1559

[84] Saintonge A., Tran K., & Holden B. P. 2008, ApJ, 685, L113

[85] Sandage A., & Visvanathan N. 1978, ApJ, 223, 707

[86] Sanders D. B., Phinney E. S., Neugebauer G., Soifer B. T., & Matthews K. 1989, ApJ, 347, 29

[87] Schechter P. 1976, ApJ, 203, 297

[88] Stern D., Eisenhardt P., Gorjian V., Kochanek C. S., Caldwell N., et al. 2005, ApJ, 631, 163

[89] Stott J. P., Smail I., Edge A. C., Ebeling H., Smith G. P., Kneib J., & Pimbblet K. A. 2007, ApJ, 661, 95

[90] Teyssier R., Moore B., Martizzi D., Dubois Y., & Mayer L. 2010, ArXiv e-prints

[93] Tran K., van Dokkum P., Franx M., Illingworth G. D., Kelson D. D., & Schreiber N. M. F. 2005a, ApJ, 627, L25

[94] Tran K., van Dokkum P., Illingworth G. D., Kelson D., Gonzalez A., & Franx M. 2005b, ApJ, 619, 134

[91] Tran K., Franx M., Illingworth G. D., van Dokkum P., Kelson D. D., Blakeslee J. P., & Postman M. 2007, ApJ, 661, 750

[92] Tran K.-V. H., Papovich C., Saintonge A., Brodwin M., Dunlop J. S., et al. 2010, ApJ, 719, L126

[95] Treu T., Ellis R. S., Kneib J., Dressler A., Smail I., Czoske O., Oemler A., & Natarajan P. 2003, ApJ, 591, 53

[96] van Dokkum P. G., Franx M., Kelson D. D., Illingworth G. D., Fisher D., & Fabricant D. 1998, ApJ, 500, 714

[97] Verdugo T., de Diego J. A., & Limousin M. 2007, ApJ, 664, 702

[98] Werner M. W., Roellig T. L., Low F. J., Rieke G. H., Rieke M., et al. 2004, ApJS, 154, 1

[99] Zhang F., Han Z., Li L., & Hurley J. R. 2004, MNRAS, 350, 710

[100] Zhang Y., Böhringer H., Mellier Y., Soucail G., & Forman W. 2005, A&A, 429, 85